Flexible Reactive Power Control in Multigroup Current-Sourced HVDC Interconnections

Nick J. Murray, *Member, IEEE*, Jos Arrillaga, *Fellow, IEEE*, Yong He Liu, *Member, IEEE*, and Neville R. Watson, *Senior Member, IEEE*

***Abstract*—Self-commutating multilevel current reinjection is a potential alternative to conventional HVDC thyristor technology. An important drawback of the multilevel configurations is the interdependence of the reactive power injections at both ends of the link. This paper describes a new concept applicable to large power converters consisting of two series-connected twelve-pulse groups. It is based on the use of a controllable shift between the firings of the two twelve-pulse groups in opposite directions, a new concept that provides independent reactive power control at the sending and receiving ends. The theory is verified by EMTDC simulation.**

***Index Terms*—HVDC transmission, multilevel conversion, reactive power control.**

NOMENCLATURE

α_{1A}, α_{1B}	Sending end converter group firing angles.
α_2	Receiving end converter firing angle.
I_1	Sending end current.
I_2	Receiving end current.
I_{1A}, I_{1B}	Sending end converter group currents.
I_{2A}, I_{2B}	Receiving end converter group currents.
P^*	Real power order.
P_1	Sending end power.
P_d	DC power.
P_{sp}	Specified power.
Q^*	Reactive power order.
Q_1	Sending end reactive power.
Q_2	Receiving end reactive power.
V_1	Sending end source voltage.
V_{1T}	Sending end converter terminal voltage.
V_2	Receiving end source voltage.
V_{2T}	Receiving end converter terminal voltage.
X_1	Sending end series reactance.
X_2	Receiving end series reactance.

I. INTRODUCTION

OWING to their structural simplicity and four quadrant power controllability, pulse width modulation (PWM) conversion has so far been the preferred option for self-commutating medium power HVDC transmission [1], [2]. However, this technology is less suited to large power ratings and long distances, due to higher switching losses and to the rating limitations of its main components (namely the power transistor switch and underground cable). Thus the interchange of large quantities of power between separate power systems and the transmission of power from remote generating stations are still based on the principle of line-commutated current source conversion.

Multilevel VSC configurations have been presented as possible alternatives [3], [4] to PWM-VSC Transmission, but their structural complexity has been the main obstacle to their commercial implementation. A recent proposal, the multilevel current reinjection (MLCR) concept [5], simplifies the converter structure and permits the continued use of conventional thyristors for the main converter bridges [6].

The main advantage of self over natural-commutation in HVDC transmission is the ability to control independently the reactive power at each end of the link, a property that can not be achieved by MLCR-based (or any other multilevel) configuration when using only one double-bridge converter group. However, interconnections of large power ratings will normally use two or more 12-pulse converter groups and these can be controlled independently from each other without affecting the output voltage waveform. This fact constitutes the basis of the new control scheme proposed here. When the operating condition at one end of the link alters the reactive power balance at this end, the firings of the two groups at the other end are shifted with respect to each other in opposite directions to keep the power factor constant. The new control concept gives the MLCR configuration described in [5] the flexibility until now only available to PWM–VSC transmission.

II. INTERDEPENDENCE OF THE REACTIVE POWER UNDER CONVENTIONAL CONTROL

PWM provides fully independent controllability of the converter voltages (and therefore reactive power transfers) on both sides of the link. This capability is not available to multilevel configurations under the present control strategies. For instance, if extra reactive power is needed at the receiving end to maintain the ac terminal voltage constant, the firing angle (α) is increased and, therefore, the dc voltage reduced. To continue transmitting the specified power under this condition, the sending end station must also reduce its dc voltage. The dc voltage reduction is implemented by a corresponding increase in the firing angle of the two converter groups; this action will force an unwanted extra injection of reactive power and, thus, an increase of ac terminal voltage at this end. Such condition would not occur if

Manuscript received April 11, 2012; revised September 24, 2012. First published December 3, 2013; current version published April 24, 2014. This work was supported by the Electric Power Engineering Centre (hosted by the University of Canterbury). Paper no. TPWRD-00186-20013.

N. J. Murray, J. Arrillaga, and N. R. Watson are with the University of Canterbury, Christchurch, New Zealand (e-mail: njm58@student.canterbury.ac.nz; arrillj@elec.canterbury.ac.nz; n.watson@elec.canterbury.ac.nz).

Y. H. Liu is with the Inner Mongolia University of Technology, Hohhot 010051, China (e-mail: ylew@imut.edu.cn).

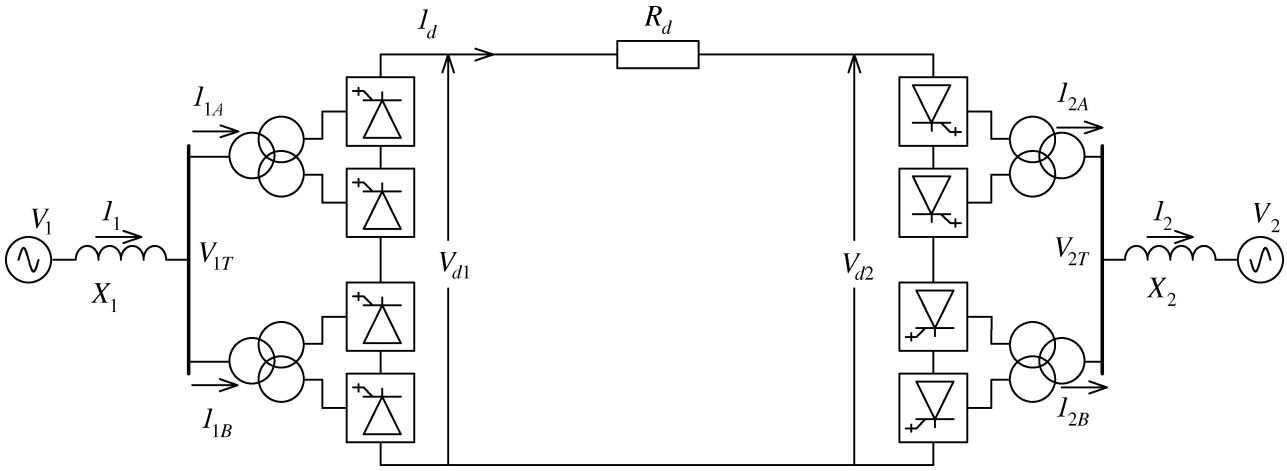

Fig. 1. Simplified diagram of a dc link connecting two ac systems.

some PWM control were to be added to the multilevel configurations. However the use of PWM is currently limited to three levels and is only used in voltage source conversion schemes.

III. Multigroup Firing-Shift Concept

The exchange of reactive power between the converter and ac system is determined by the sine of the firing angle (α). Altering (α) has an immediate effect on the dc voltage level and, thus, to maintain the specified dc power transfer through the link, a corresponding change of firing angle must be made at the other end, which in turn affects its reactive power exchange with the ac system. Therefore, under conventional converter control, the reactive powers injected at the two ends of a multilevel CSC link are interdependent.

In multilevel CSC HVDC interconnections with two twelve pulse groups per terminal (such as shown in Fig. 1) the same current waveform is produced by each of the 12-pulse converter groups, and thus the total output current waveform remains the same if a phase-shift is introduced between the firings of the two groups constituting the converter station.

When a change of operating conditions at the receiving end demands more reactive power from the converter, and thus reduces the dc voltage, shifting the firings of the two sending end converter groups in opposite directions provides the required dc voltage reduction, while maintaining the reactive power constant (due to the opposite polarity of the two firing angle corrections). A relatively small change of active power will be caused by the variation of the fundamental current produced by the shift, but this change can be compensated for by a small extra correction of the two firing angles.

For a converter to operate in the firing-shift mode (which in the above example is the sending end converter), the firing instants of one group (say group A) is kept on the positive side (thus providing reactive power), while the second group (say group B) may act as a source or sink of reactive power (i.e., the firing angle may be positive or negative).

A. Steady State Operation

To simplify the explanation of the steady state characteristics only, the sending end operates under firing shift control, while the receiving end uses a common firing angle for the two converter groups. The generalized method with firing shift at both ends will be used in the dynamic simulation.

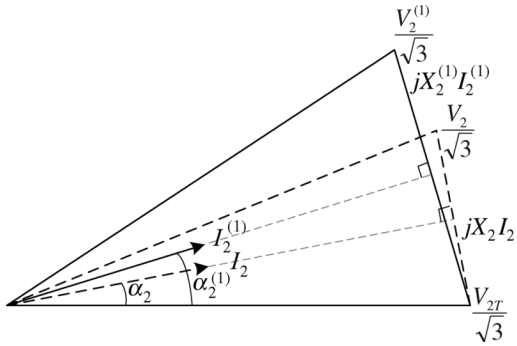

Fig. 2. Operating conditions at the receiving end for two different system strengths.

Also, as shown in Fig. 1, the interconnected ac systems are represented as simplified Thevenin equivalents, i.e., V_1, X_1 and V_2, X_2.

At the receiving end the control specifications are the terminal ac voltage (V_1) and the dc voltage (V_d), while those at the sending end are the dc power transfer (P_{d1}^{sp}) and the reactive power (Q_1).

Receiving end:

As at this end no firing shift control is exercised, the firing angle will be the same for the two converter groups (i.e., $\alpha_{2A} = \alpha_{2B} = \alpha_2$).

The dotted lines in the phasor diagram of Fig. 2 represent the initial operating condition (with a Thevenin impedance of X_2) and the continuous line a new operating condition with a larger Thevenin impedance $(X_2^{(1)})$.

In both cases, the system reactive power requirements are equally shared between the converter and the ac source with the same firing angle used in both converter groups.

The condition is represented by the following equations:

$$I_{2A} = I_{2B} = k_m I_d \tag{1}$$

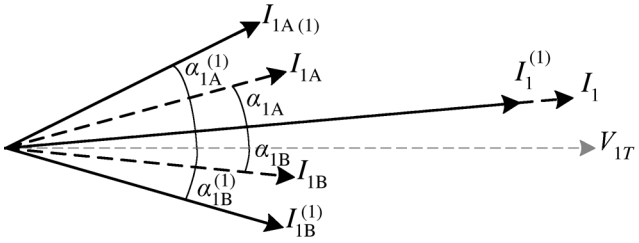

Fig. 3. Firing shift control maintaining constant reactive power at the sending end for two different system strengths.

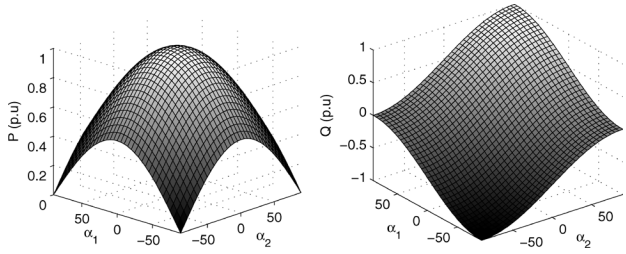

Fig. 4. Calculated real and reactive power for varied firing angle ($\pm 90°$).

or between the double converter ac and dc currents

$$I_2 = 2k_m I_d \quad (\text{where } k_m = 1.59) \tag{1a}$$

and

$$\left(\frac{V_2}{\sqrt{3}}\right)^2 - \left(\frac{V_{2T}}{\sqrt{3}}\right)^2 = X_2^2 I_2^2 - 2\left(\frac{V_{2T}}{\sqrt{3}}\right) XI\sin(\alpha_2) \tag{2}$$

$$V_{d2} = 4\left(\frac{3\sqrt{2}}{\pi}\right) V_{2T}\cos(\alpha_2). \tag{3}$$

In terms of the specified power (which is normally controlled at the sending end) the dc voltages across the link are related by the expression

$$V_{d1} = V_{d2} + R_d \frac{P_{d1}^{sp}}{V_{d1}}.$$

Or making $\mathrm{V_{d1}}$ the subject and taking the positive root

$$V_{d1} = \frac{V_{d2} + \sqrt{V_{d2}^2 + 4R_d P_{d1}^{sp}}}{2}. \tag{4}$$

The solution of (1a)–(4) provides the initial values of α_2, V_{d2}, V_{d1}, I_2.

Sending end:

Fig. 3 illustrates the two operating conditions in response to the change at the receiving end. Initially the sending end is set with one firing angle positive and one negative to demonstrate the phase shift control principle, these are represented by α_{1A} and α_{1B}. When a change in operating conditions occurs, as a result of an increased Thevenin impedance and, thus, of firing angle at the receiving end, the sending end must compensate by an increase in firing angle ($\alpha_{1A}^{(1)}$ and $\alpha_{1B}^{(1)}$ in Fig. 3) to maintain the specified active power transfer.

The following relationships apply to the sending end:

$$V_{d1} = 2\left(3\frac{\sqrt{2}}{\pi}\right) V_{1T}\left(\cos(\alpha_{1A}) + \cos(\alpha_{1B})\right) \tag{5}$$

$$I_{1A} = k_m I_d \tag{6}$$

and shown in the equation at the bottom of the page or, because $|I_{1A}| = |I_{1B}|$ due to the series connection

$$I_1 = \sqrt{2} I_{1A}\sqrt{1+\cos(\alpha_{1A}-\alpha_{1B})} = 2I_{1A}\cos\left(\frac{(\alpha_{1A}-\alpha_{1B})}{2}\right). \tag{7}$$

The active power P_1 is equal to the specified dc power P_{d1}^{sp}

$$P_1 = V_{1T} I_{1A}\left(\cos(\alpha_{1A}) + \cos(\alpha_{1B})\right) \tag{8}$$

and the reactive power

$$Q_1 = V_{1T} I_{1A}\left(\sin(\alpha_{1A}) + \sin(\alpha_{1B})\right). \tag{9}$$

With V_1, V_{1T}, and P_1 specified, the unknown variables are V_{d1}, I_{1A}, I_1, α_{1A}, α_{1B}, Q_1, which can be derived from the simultaneous solution of (4)–(9).

In the steady state, the values of α_{1A}, α_{1B} and, thus, the internal reactive power circulation between the two converter groups, can be reduced by the use of the transformer on load tap change.

IV. Control Structure

For complete flexibility the sending end needs to control real and reactive power and the receiving end keep the converter dc voltage constant (so as to minimize dc current for a given real power setting) and control the reactive power. With reactive power control at both ends, the controllers can easily be configured for optimum power transfer at the system level depending on operating objectives, which usually involves providing constant power factor at the sending end and constant ac terminal voltage at the receiving end.

In order to control the real and reactive power over the complete operating range the converter response needs to be linear. Standard PID controllers are unsuitable for this application as their gain is static, and although they may give suitable performance over a narrow band, the latter is not acceptable over the complete range. This is explained in more detail later.

Fig. 4 illustrates the control ranges of the real and reactive power responses for a values of $\pm 90°$. It is clear that these controller surfaces are very nonlinear, and it is not hard to understand why a linear PID controller would be unsuitable.

$$I_1 = \sqrt{\left(I_{1A}\cos(\alpha_{1A}) + I_{1B}\cos(\alpha_{1B})\right)^2 + \left(I_{1A}\sin\alpha_{1A}) + I_{1B}\sin(\alpha_{1B})\right)^2}$$

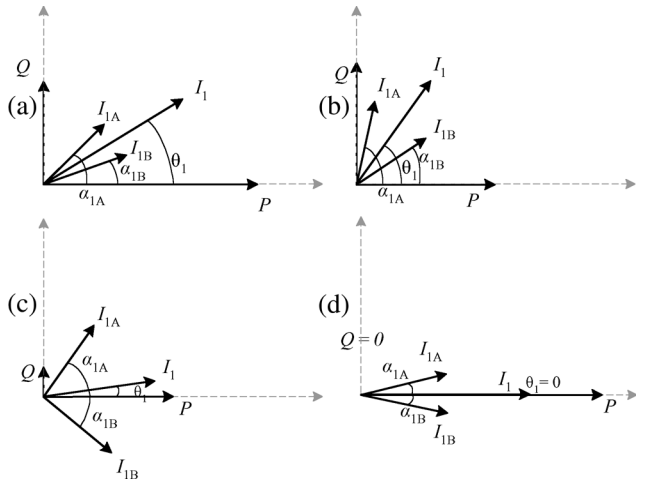

Fig. 5. Firing shift control providing (a) large P and Q, (b) large Q and smaller P, (c) small P and Q, and (d) large P, no Q.

Given the aforementioned controller surfaces, it is difficult to visualize how the controller must perform, especially since the controller firing angles are expected to operate equally well in the positive and negative regions. What is needed is a controller that operates for all combinations of P and Q without the need to manually switch controller gains and control actions. An example of four controller operating conditions is shown in Fig. 5.

These diagrams show that the controller is expected to operate over a wide range of conditions and that the change in firing angle has the greatest influence on the real power near the X axis and on the reactive power near the Y axis. This is better explained by examining the real and reactive power contribution of one converter in isolation. The real power transferred by the converter depends on the cosine of the firing angle (α_1) while the reactive power depends on the sine of (α_1). What is of interest to control system designers is the rate of change of the controlled outputs P and Q, as this determines the level of gain (or sensitivity) in system response. Basic differentiation reveals that the rate of change is proportional to $-\sin(\alpha_1)$ for real power and to $\cos(\alpha_1)$ for reactive power, which makes this system very nonlinear.

As mentioned earlier, conventional controller operation is confined to a relatively small range and functions with a fixed gain, thereby assuming that the system is linear over the small range. This control philosophy becomes even less suitable when we consider that an ideal independent and fully flexible controller should be able to provide a combination of (α_1) and (α_2) that satisfies the requirements of both P and Q simultaneously.

Fig. 6 illustrates a simplified block diagram of what the controller must achieve, the goal being a mapping function that translates P and Q into α_1 and α_2, to make the nonlinear converter appear linear. In doing this, then linear control theory may be used successfully.

The only information representing the behavior of the converter system is given by the steady state (8) and (9), but this is sufficient initially, because they show the influence that $\Delta\alpha_1$ and $\Delta\alpha_2$ have on the output variables P and Q.

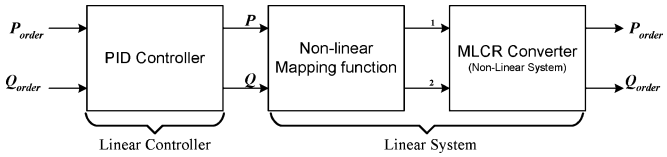

Fig. 6. Block diagram of the nonlinear system control objective.

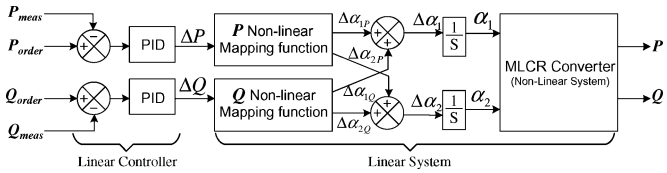

Fig. 7. Implementation of nonlinear control theory.

The rate of change of the output variables with respect to firing angles α_1 and α_2 can be expressed as

$$\Delta P = \frac{\partial P}{\partial \alpha_1}\Delta\alpha_1 + \frac{\partial P}{\partial \alpha_2}\Delta\alpha_2 \tag{10}$$

$$\Delta Q = \frac{\partial Q}{\partial \alpha_1}\Delta\alpha_1 + \frac{\partial Q}{\partial \alpha_2}\Delta\alpha_2. \tag{11}$$

These are found by differentiating the steady state (8) and (9), i.e.,

$$\frac{\partial \mathbf{P}}{\partial \alpha_1} = -3V_T I_1 \sin(\alpha_1) \tag{12}$$

$$\frac{\partial \mathbf{P}}{\partial \alpha_2} = -3V_T I_1 \sin(\alpha_2) \tag{13}$$

$$\frac{\partial \mathbf{Q}}{\partial \alpha_1} = 3V_T I_1 \cos(\alpha_1) \tag{14}$$

$$\frac{\partial \mathbf{Q}}{\partial \alpha_2} = 3V_T I_1 \cos(\alpha_2). \tag{15}$$

Expressing the dynamic system in matrix form

$$\begin{bmatrix}\Delta P \\ \Delta Q\end{bmatrix} = \underbrace{\begin{bmatrix}\frac{\partial \mathbf{P}}{\partial \alpha_1} & \frac{\partial \mathbf{P}}{\partial \alpha_2} \\ \frac{\partial \mathbf{Q}}{\partial \alpha_1} & \frac{\partial Q}{\partial \alpha_2}\end{bmatrix}}_{A} \begin{bmatrix}\Delta\alpha_1 \\ \Delta\alpha_2\end{bmatrix}. \tag{16}$$

Equation (16) can be solved using basic matrix theory.

Using the partial differentials of the steady state equations to P and Q in Matrix A, it is possible to model the converter systems transient response (but not the system state).

If the matrix is nonsingular, its inverse can be used to linearize the converter system behavior. The inverse of Matrix A, with the common gain component grouped on the left side, becomes

$$A^{-1} = \frac{1}{3V_T I_1 \sin(\alpha_1 - \alpha_2)} \begin{bmatrix}-\cos(\alpha_2) & -\sin(\alpha_2) \\ \cos(\alpha_1) & \sin(\alpha_1)\end{bmatrix}. \tag{17}$$

This equation indicates that the overall system gain depends on the difference between the two firing angles $(\sin(\alpha_1 - \alpha_2))$ and the contribution of (for P) real power on the other groups firing angle, and (for Q) reactive power contribution on the other groups firing angle. While making sense in theory, this needs to be realized in practice.

Examining the system on an incremental basis (i.e., from $\alpha_1 \rightarrow \alpha_1 + \delta\alpha_1$), as the difference $(\delta\alpha_1)$ is reduced, the ac-

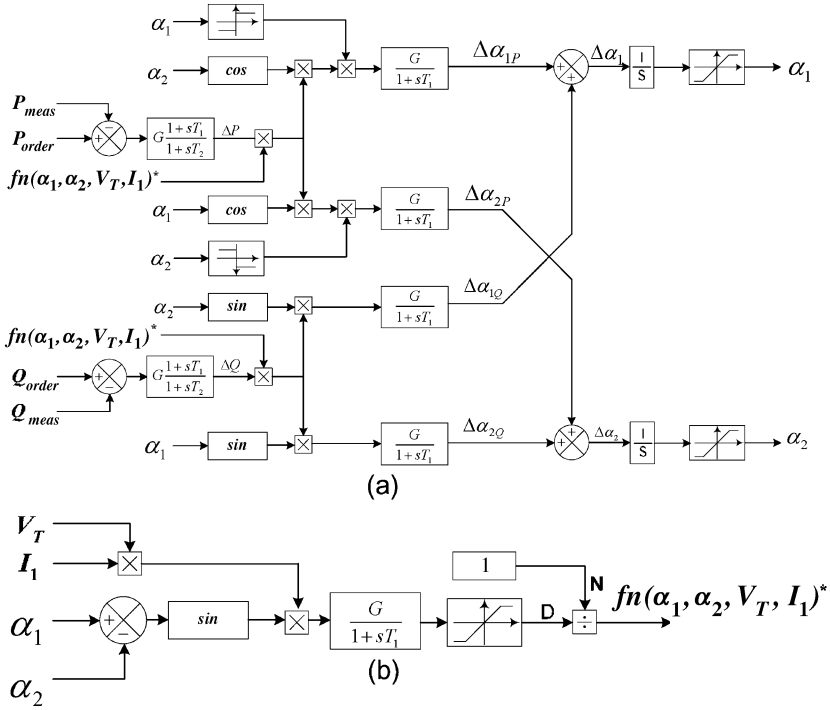

Fig. 8. Sending end controller block diagram, with the main linearizing components in (a) and the common angle difference calculation in (b).

curacy is increased, becoming very close to the continuous integral equivalent. It could be argued that in each partial differential equation, the effect of $\Delta\alpha_1$ on $\Delta\alpha_2$ and vice versa is not fully captured, but in a practical system this effect can be minimized with suitable feedback

A. Practical Implementation

Figs. 7 and 8 show the implementation of the theory into a real system controller.

In Fig. 7, the controller has two separate channels, one for each of the P and Q components. For each channel, the theory is the same; the error is calculated by subtracting the measured power from the power order, and this is fed into the PID controller. The increment of ΔP and ΔQ becomes the input into the nonlinear mapping function, which resolves the increment of ($\Delta\alpha_{1\mathrm{P}}$ and $\Delta\alpha_{2\mathrm{P}}$), and ($\Delta\alpha_{1\mathrm{Q}}$ and $\Delta\alpha_{2\mathrm{Q}}$) from the P and Q channels, respectively. The nonlinear errors are combined and then $\Delta\alpha_1$ and $\Delta\alpha_2$ are integrated to provide the required outputs (α_1) and (α_2) as inputs into the converter firing logic.

The nonlinear mapping function in Fig. 7 for P is represented by A_{11}^{-1}, A_{21}^{-1}, and for Q is A_{12}^{-1}, A_{22}^{-1} in (17).

Fig. 8 shows how the system is realized in a practical controller. The controller layout follows almost exactly the analytical development from (10)to (17), with only additional low-pass filters added to prevent ringing when the error is almost zero. It is important to note that the common component of the converter control is calculated separately [Fig. 8(b)], since this determines the overall gain of the system. Hard limits on the calculation are provided so as to prevent wind up and instability which can occur if $\alpha_1 = \alpha_2$. Also to ensure that firing angle α_1 is always greater than α_2, limits are placed on the integrators.

The receiving end controller topology is much the same as that of the sending end, but as it must control Vdc_r and Q_r, the layout is different. Using steady state (5) and (9), the inverse transfer function becomes

$$A^{-1} = \frac{1}{3V_T \sin(\alpha_1 - \alpha_2)} \begin{bmatrix} \frac{-\sqrt{2}\pi\cos(\alpha_2)}{4} & \frac{-\sin(\alpha_2)}{I_1} \\ \frac{\sqrt{2}\pi\cos(\alpha_1)}{4} & \frac{\sin(\alpha_1)}{I_1} \end{bmatrix}. \quad (18)$$

Given the steady-state equations and taking into consideration (6), it becomes apparent that although full control is justified by the theory, the range of Q control depends on the magnitude of I_{dc}. Optimum dc power transmission occurs when the dc current is minimized, as this also minimizes the dc link power losses; however this affects the range of Q controllability at both the sending and receiving ends. As the reactive power circulation is confined to the ac system side, the magnitude of the ac current in each converter group determines the level of reactive power controllability in the ac system. The real power, which is also a function of the ac current magnitude, is determined by the combination of V_{dc} and I_{dc} on the dc link. To understand the reactive power controllability limits, it must be realized that the same amount of real power can be transferred with a combination of high V_{dc}/low I_{dc}, or low V_{dc}/high I_{dc}.

An example of this in a multigroup MLCR, in per unit terms is given

$$\text{High } V_{dc}: \; Pdc = 1pu = 5.5puV_{dc} \times 0.182puI_{dc} \quad (19)$$

$$\text{Low } V_{dc}: \; Pdc = 1pu = 2.25puV_{dc} \times 0.364puI_{dc} \quad (20)$$

and so with $I_1 = \sqrt{3}k_m I_{dc}$ and V_{ac} being the same in both cases, (9) shows that (20) would yield twice the reactive power for a given firing angle as (19).

So with conflicting objectives in real power efficiency and reactive power controllability, a compromise must be made between control range and overall efficiency during system design.

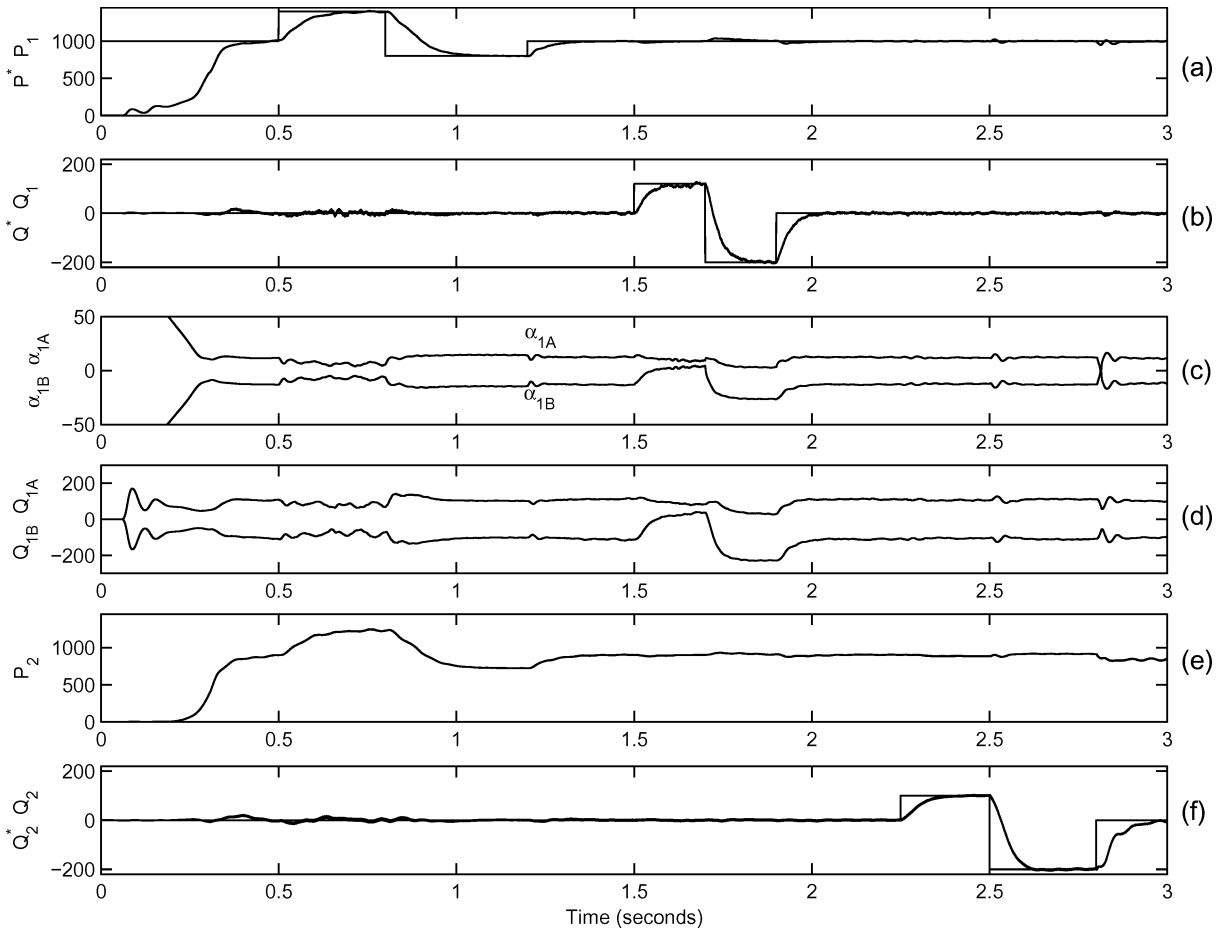

Fig. 9. Real and reactive power order changes at the sending and receiving ends.

V. Dynamic Simulation

A. Test System

The test circuit is a simplified HVDC link configuration with the two interconnected systems represented as Thevenin equivalents. As shown in Fig. 1, each terminal consists of two five-level MLCR converter groups.

Using 1000 MW and 220 kV as base values, the source voltages are set at 1.06 and 1.02 p.u. at the sending and receiving ends, respectively. The series impedances at the sending and receiving ends are set to 0.2 p.u. to represent systems with SCRs of approximately 3.1, and the transformer leakage reactance of all converter transformers is equal to 0.1 p.u. The dc line is represented by a resistance of 0.2 p.u. in series with a 2H smoothing inductor. The active power transfer and reactive power are the controlled variables at the sending end; at the receiving end the controlled variables are the dc voltage and the reactive power order.

B. Simulation Verification and Reactive Power Independence

The test system has been modelled using the PSCAD/EMTDC package and the response to a series of step changes over a 3-s period are presented in Fig. 9.

Changes in the active power order from 1000 to 1400 MW (at 0.5 s) and from 1400 to 800 MW (at 0.75 s) are shown in Fig. 9(a); their effect on the reactive power at either end of the link is shown in graphs (b) and (f) to be negligible.

Likewise, Fig. 9(b) shows step changes in the reactive power order at the sending end, first from 0 to $+100$ MVAr (at 1.5 s) and later from $+100$ to -200 MVAr (at 1.7 s); the effect on the receiving end active and reactive power (shown in graphs (e) and (f), respectively) are also negligible and they only cause a slight disturbance to the active power at the sending end [as shown in graph (a)].

The effect of the above changes on the group firings at the sending end, illustrated in graph (c), show that a1B can operate with positive and negative values, thereby minimizing the reactive power circulation between the groups [clearly noticeable between 1.5 and 1.7 s in graph (d)]. Fig. 9(f) shows a change in the reactive power order at the receiving end, from 0 to 100 MVAr (at 2.25 s) and from 100 to -200 MVAr (at 2.5 s). These produce a small change of active power, which requires a small correction in the firing angle, but no visible change is observed in the sending end reactive power [graph (b)].

As the secondary control objective is to maintain dc voltage constant, a maximum step of $+100$ MVAr is possible at the receiving end. This is because the receiving end terminal voltage decreases as more reactive power is required by the converter, which further contributes to the decrease in dc voltage for a given firing angle.

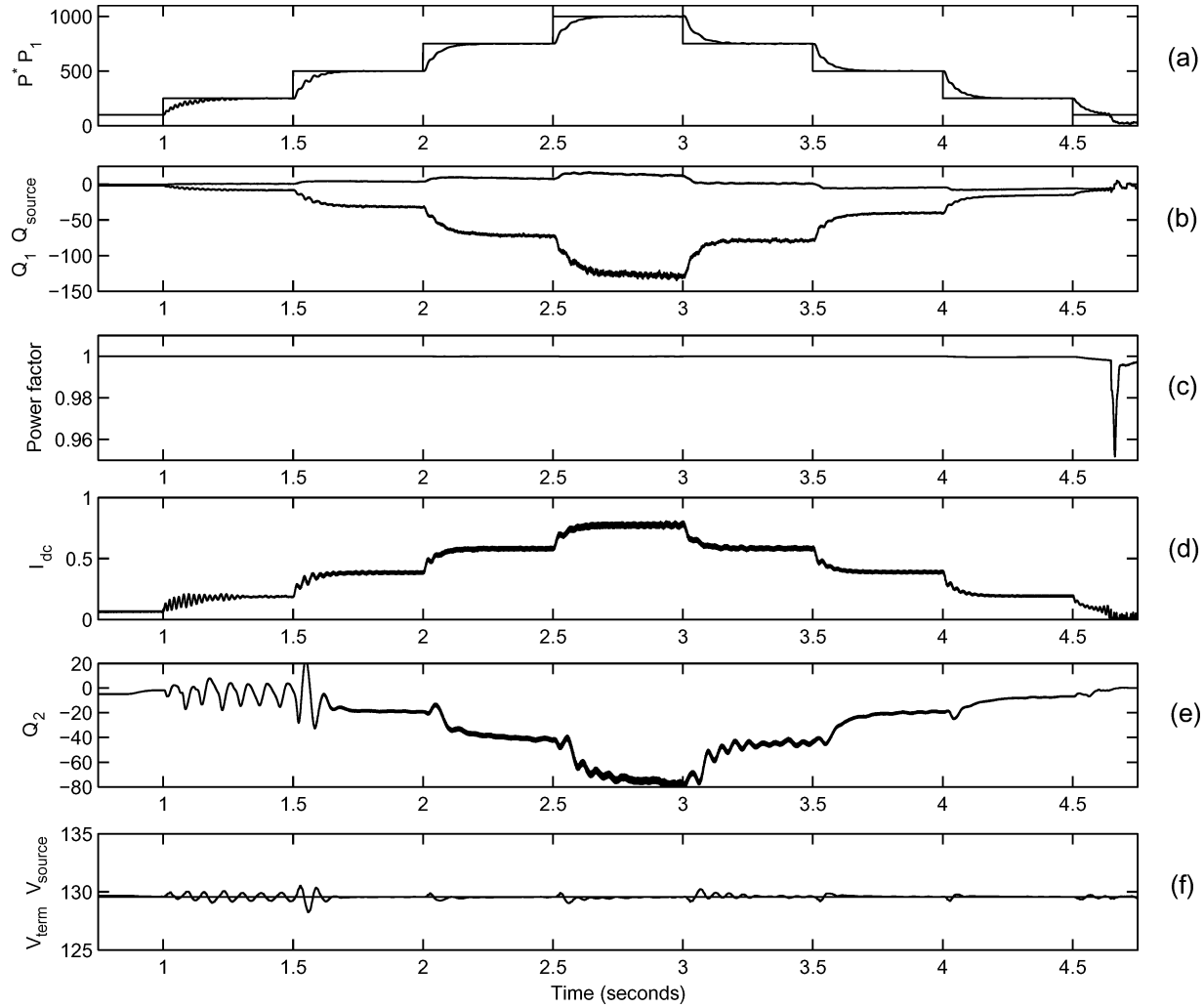

Fig. 10. Reactive power responses under power factor and terminal voltage control for a series of step changes to real power.

C. Simulation of Unity Power Factor and Constant Terminal Voltage Operation

The dynamic simulation in PSCAD/EMTDC features the effect of four separate controllers, one for each of the reactive powers, and one for the sending end real power and receiving end dc voltage. By adding an extra controller to each of the reactive power orders, it is possible to control the system to provide unity power factor and constant terminal voltage over the complete real power operating range.

The sending end correction is made from the point of view of the ac system, so the converter controller is configured to maintain the power factor of the main supply transmission line as well. In practice it may not be possible to calculate the impedance of the supply in all cases, and an approximation would have to be made about a "nominal" correction point.

At the receiving end, the control of the terminal voltage should be easier to achieve, as the nominal supply voltage would be known, or could be calculated. This could also be adjusted manually by the system operator to provide additional voltage support as necessary.

Fig. 10(a)–(f) presents an example of the multigroup MLCR dc link providing power factor correction and terminal voltage control. To highlight the dynamics of the control method, the real power order is modified in (a) in a series of steps, as listed

Steps 1 & 7	250 MW
Steps 2 & 6	500 MW
Steps 3 & 5	750 MW
Steps 4	1000 MW
Steps 8	0 MW.

The reactive power responses are plotted in Fig. 10(b) and (e) for the sending and receiving ends, respectively, and the sending end power factor in (c). In (f), the constant line represents the receiving end source, and the second line is the terminal voltage.

It is important to note in (e) and (f), that under this control scheme (i.e., with optimized Vdc) for real power transfers of 250 and 500 MW, the ac current at the receiving end is insufficient to provide stable terminal voltage control. This highlights one of the limitations of maximizing Vdc; although, however, this can be easily corrected by reducing Vdc during situations where low real power transfer is required.

VI. Conclusion

A new type of converter control has been developed, applicable to multilevel HVDC schemes with two or more 12-pulse

groups per terminal. It has been shown theoretically, and verified by EMTDC simulation using an MLCR configuration, that the use of a controllable shift between the firings of the series-connected converter groups permits independent reactive power control at the two dc link terminals. This provides four quadrant power controllability to multilevel current source HVDC transmission and, thus, makes this alternative equally flexible to PWM-controlled voltage source conversion, without the latter's limitations in terms of power and voltage ratings. It can be expected that MLCR, combined with firing-shift control, should compete favorably with the conventional current source technology for very large power applications.

REFERENCES

[1] G. Asplund, K. Eriksson, and O. Tollerz, "Land and sea cable interconnections with hvdc light," presented at the CEPSI Conf., Manila, Philippines, Oct. 2000.

[2] G. Asplund, K. Eriksson, and K. Svensson, "DC transmission based on voltage source converters," presented at the CIGRE SC Colloq., Johannesburg, South Africa, 1977.

[3] Cigre SC-4 WG 37, VSC Transmission Final document. Paris, France, 2004.

[4] G. Jung *et al.*, "A general circuit topology of multilevel inverter," in *Proc. IEEE Power Electronics Specialist Conf.*, 1991, vol. PESC 91 Rec., pp. 96–103, Mass. Inst. Technol..

[5] L. B. Perera, N. R. Watson, Y.-H. Liu, and J. Arrillaga, "Multi-level current reinjection self-commutated HVDC converter," *Proc. Inst. Elect. Eng., Gen., Transm. Distrib.*, vol. V152, no. 5, pp. 607–615, Sep. 2005.

[6] J. Arrillaga, Y. H. Liu, L. B. Perera, and N. R. Watson, "A current reinjection scheme that adds self-commutation and pulse multiplication to the thyristor converter," *IEEE Trans. Power Del.*, vol. 21, no. 3, pp. 1593–1599, Jul. 2006.

Nick J. Murray (M'07) received the B.E. (Hons.) degree in electrical and electronic engineering from the University of Canterbury, Christchurch, New Zealand, in 2001, where he is currently pursuing the Ph.D. in flexible reactive power control in HVDC converters.

Jos Arrillaga (F'91) received the B.E. degree in Spain and the M.Sc., Ph.D., and D.Sc. from the University of Manchester Institute of Science and Technology (UMIST).

Currently, he is a Professor at the University of Canterbury, Christchurch, New Zealand, where he has been since 1975. He is a Fellow of the IEE and of the Royal Society of New Zealand.

Yonghe He Liu (M'03) received the M.E. degree in automation from The Chinese Science Academy and the Ph.D. degree from the University of Canterbury, Christchurch. New Zealand.

Currently, he is a Professor at the Inner Mongolia University of Technology, Hohhot, China

Neville R. Watson (SM'89) received the B.E. (Hons.) and Ph.D. degrees in electrical engineering from the University of Canterbury, Christchurch, New Zealand.

Currently, he is an Associate Professor with the University of Canterbury. His interests include steady-state and dynamic analysis of ac/dc power systems.